# Effect of dipolar interaction observed in iron-based nanoparticles

J. M. Vargas,[1,2,*] W. C. Nunes,[2] L. M. Socolovsky,[2] M. Knobel,[2] and D. Zanchet[1]
[1]*Laboratório Nacional de Luz Síncrotron, Giuseppe M. Scolfaro 10000, Campinas (SP) 13084-971, Brazil*
[2]*Instituto de Física "Gleb Wataghin", Universidade Estadual de Campinas, Campinas (SP) 13083-970 Brazil*
(Received 1 April 2005; revised manuscript received 18 August 2005; published 23 November 2005)

Spherical magnetic nanoparticles with narrow size distribution and organic capping were diluted in paraffin with different concentrations to verify the role of dipolar interactions on the macroscopic magnetic behavior. Increasing concentration of magnetic nanoparticles leads to higher blocking temperatures. The experimental data were analyzed by means of a recently proposed model that takes into account magnetic interactions of dipolar origin, and an excellent agreement was found. Considering the magnetic interaction among particles it was possible to obtain the real magnetic moment and estimate structural parameters that are consistent with the ones obtained by small angle x-ray scattering and transmission electron microscopy.

DOI: 10.1103/PhysRevB.72.184428 PACS number(s): 75.50.Tt, 75.20.−g, 75.75.+a

## I. INTRODUCTION

A superparamagnetic system is composed by magnetic monodomain nanoparticles whose atomic magnetic moments rigidly align through exchange interaction. All the individual magnetic moments add to form a magnetic supermoment, usually of the order of thousands of Bohr magnetons ($\mu_B$). The canonical description of superparamagnetism, following the Langevin formalism, considers a negligible anisotropy for each particle and neglects the effect of interparticle interactions, which can manifest through exchange, indirect exchange, Ruderman-Kittel-Kasuya-Yosida (RKKY), or even dipole-dipole interactions.[1–3]

Although many nanostructured systems (i.e., systems with particle sizes of the order of nanometers) have been reported as superparamagnetic, a lack of agreement is commonly observed between experimental data and the standard superparamagnetic theory. These differences are usually ascribed to the intrinsic particle size distribution, anisotropies of different origins, and interactions among magnetic particles. One significant difference appears when particle size distribution functions obtained from apparently good fits performed using a weighted sum of Langevin functions are compared to the ones obtained from direct structural data, such as transmission electron microscopy (TEM) images.[4,5] Besides the lack of agreement, usually the fitted mean magnetic moment strongly increases with increasing temperature, a fact that confirms the spurious nature of the obtained parameters.[4–6] Such unusual behavior has been also observed in antiferromagnetic particles, and an alternative theoretical model based on the existence of a thermally activated surface net magnetic moment has been recently proposed to explain such a trend in those nanoparticles, but it remains controversial.[7,8]

Extensive experimental and theoretical works agree that the interaction among magnetic particles play a fundamental role in the magnetic behavior of granular systems.[8–14] However, several inconsistencies have been discussed since the late 1980s, trying to conciliate theory and different experimental data. For instance, in the limit of weak interactions, an increase of the blocking temperature with particle density has been observed in some experiments,[9,10] but other results show the opposite trend.[11] For high density particle systems, the picture is more complex since the blocking process of each nanoparticle is highly dependent on its neighborhood. The observation of properties resembling spin glasses has suggested the existence of a spin glasslike state or magnetic order in such systems. Nonetheless, most results have also been explained by progressive blocking of independent particles, leading to an intensive debate in the last years.[12–16]

In the effort to better understand this complex issue, a recent study took into account the dipolar interactions by introducing a phenomenological temperature, $T^*$, in the argument of the Langevin function, which has been known as the $T^*$ model.[4] This assumption considers that dipolar interactions tend to increase the orientational disorder of the magnetic moments, so that thermal agitation would be somewhat "enhanced" owing to dipolar interactions.

Undoubtedly, a major challenge to better understand the magnetic interactions in nanosystems and test the existing models is to produce good quality samples. In fact, the limited knowledge of nanoparticle shape, composition gradient, size distribution, or even touching nanoparticles can prevent having an accurate picture of the whole system. We have contributed to overcoming this problem by producing nanosized iron-based nanoparticles of approximately spherical shape and narrow size distribution by colloidal methods. The presence of organic, insulating capping on the surface of the magnetic particles prevents the formation of agglomerates or chains, leading to pure dipolar interactions. Furthermore, the strength of the dipolar interaction among particles can be tuned by diluting the same sample in different amounts of paraffin, allowing one to systematically study just the effect of dipolar interactions, avoiding variations in chemical composition, size distribution, and magnetic anisotropy among samples.

## II. EXPERIMENTAL PROCEDURE AND SAMPLES

Magnetic iron-based nanoparticles were prepared by colloidal synthesis (see further details in Ref. 17) and well-characterized by TEM and small angle x-ray scattering

 ©2005 The American Physical Society

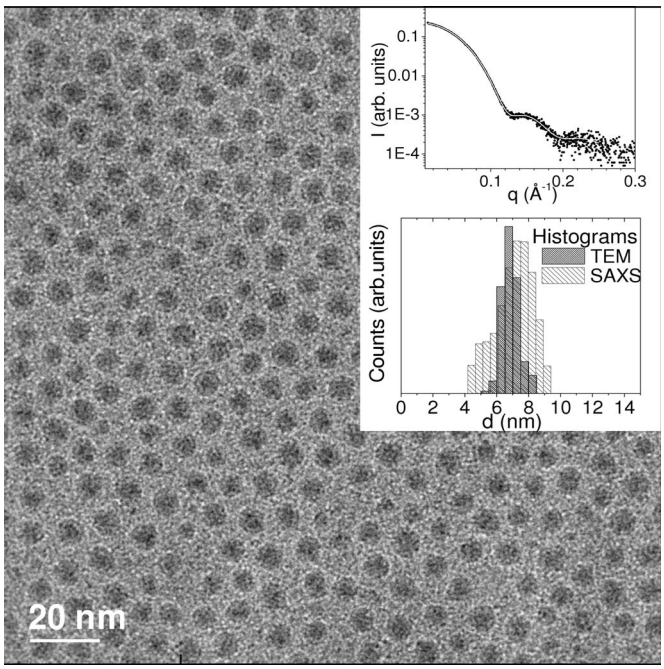


FIG. 1. A TEM image of the nanoparticle sample used in this work. The insets show the SAXS curve of the same sample (the fit is represented by the white line) and the distribution of sizes obtained from both techniques.

(SAXS). The results of both analyses are shown in Fig. 1. The TEM image shows spherical nanoparticles with mean diameter, $d_{av}$=7.1 nm and very narrow size distribution ($\sigma$ =0.08). This result is corroborated by the SAXS data of the same sample, which shows an oscillatory behavior typical of narrow size distribution spherical particles (inset of Fig. 1). SAXS data treatment was done using the GNOM program,[18] for which a sphere distribution was assumed. The SAXS analysis gave $d_{av}$=7.3 nm, similar to TEM, but a larger size distribution ($\sigma$=0.17). The distribution of particle sizes obtained by TEM and SAXS are shown in the inset of Fig. 1. It is important to point out that the difference found between the size distributions obtained by TEM and SAXS is not surprising for this kind of sample. It is known that during the solvent evaporation on the TEM grid the nanoparticles self-assemble forming large ordered regions of particles of similar sizes, excluding the smaller ones to the edges.[19] This may underestimate the TEM size distribution width. In this work we have used the size distribution obtained by SAXS since it gives an average signal and we consider that it better describes the actual system. In the following analysis, the SAXS distribution of particle sizes has been converted to a volume distribution and fitted with a Gaussian function, given a volume distribution of $\sigma_V$=0.38.

The as-synthesized nanoparticles are mainly composed by amorphous Fe and capped by oleyl-sarcosine molecules, which avoid agglomeration. The colloidal solution can be precipitated using methanol or ethanol and easily redispersed in toluene or Decalin. The slow oxidation process leads to a disordered Fe oxide, whose majority magnetic phase locally resembles magnetite ($Fe_3O_4$), as identified by Mössbauer spectroscopy.[17] To evaluate the dipolar magnetic interaction

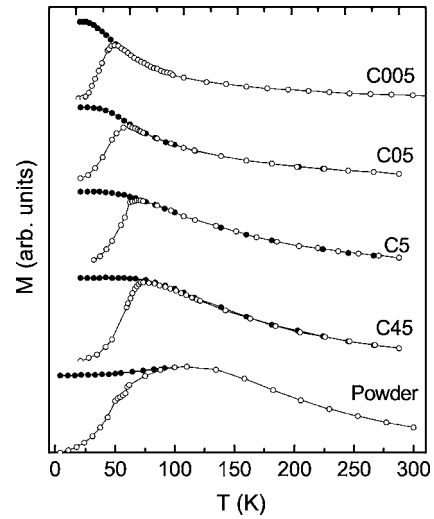


FIG. 2. The ZFC-FC curves as a function of nanoparticle concentration ($H$=20 Oe). Note that the blocking temperature clearly shifts to higher values when nanoparticle concentration increases. The irreversibility region in the FC curves shows qualitatively the increase of the dipolar interaction for higher nanoparticle concentration.

in this system, some quantity of the same batch of the colloidal solution was precipitated (powder sample) or diluted in paraffin, in different concentrations. This strategy was adopted to minimize little variations that may occur when using different batches of samples or due to the oxidation process. The dilutions used in this work were 0.05, 0.5, 5, and 45 % mass of colloid/mass of paraffin, hereinafter named C005, C05, C5, and C45, respectively. However, it is important to point out that the absolute values are just indicative of the degree of concentration due to the intrinsic large errors in the determination of the actual magnetic nanoparticle core mass.

Zero-field-cooled (ZFC) and field-cooled (FC) magnetization and magnetization vs applied field ($M$ vs $H$) measurements (magnetization loops) were performed in a commercial superconducting quantum interference device (SQUID) magnetometer (quantum design MPMS XL7). The diamagnetic contribution of the paraffin was subtracted from the magnetization data and the results were presented in the reduced form for all samples, i.e., $M/M_S$ vs $H$, to avoid misleading results due to the uncertainties in the nanoparticle mass determination.

## III. RESULTS AND DISCUSSION

### A. Magnetic properties

ZFC and FC curves as functions of particle concentration are shown in Fig. 2 ($H$=20 Oe). As can be clearly seen, for increasing particle concentration the splitting points between ZFC and FC curves as well as the maxima of the ZFC curves shift to higher temperatures, indicating an increase in the blocking temperature, $T_B$.[20] A similar trend was previously observed by Dormann *et al.*, Zysler *et al.*,[21,22] and in Monte Carlo simulations,[23,24] for example. Such results qualitatively

agree with the Dormann-Bessais-Fiorani model.[9] Also, the FC magnetization curvature in the irreversibility region (below blocking temperature) qualitatively marks the strength of interparticle interaction, diminishing its relative height with respect to the maximum of the ZFC curve as the concentration increases. It is worth mentioning that the overall shape of the ZFC curves for all samples is similar, indicating that no percolation occurs among particles, so reassuring that the magnetic properties can be, in principle, described in the framework of the superparamagnetic model. In some systems composed by nanoparticles, when the volume concentration of the magnetic element reaches 17–25 %, a clear distinctive shape of the ZFC curve appears due to direct contact among magnetic nanoparticles.[25,26]

It is known that the ZFC curve is sensitive to the distribution of activation energy ($25\ kT_B$) that can be easily calculated considering a system of noninteracting particles with $x$ volume concentration of particles.[20] For a single particle of volume, $V$, the magnetization, $M$, under low magnetic field, $H$, is expressed as $M=(M_S^{\text{core}})^2\ VH/kT$ in the superparamagnetic region ($T>T_B$), and $M=(M_S^{\text{core}})^2\ H/3$ K in the blocked region ($T<T_B$), respectively ($T$ is the system temperature, $M_S^{\text{core}}$ is the saturation magnetization of the nanoparticle magnetic core, $k$ is the Boltzmann constant, and $K$ is the anisotropy constant). Therefore, for a noninteracting fine particle system the total magnetization can be written as[27]

$$\frac{M_{ZFC}(H,T)}{M_S} = \frac{M_S^{\text{core}}H}{3K}\int_{V_b(T)}^{\infty} f(V)dV + \frac{M_S^{\text{core}}H}{3kT}\int_0^{V_b(T)} Vf(V)dV, \qquad (1)$$

where $V_b(T)=25kT/K$, and $f(V)$ is the particle volume distribution, and $M_S$ is the sample saturation magnetization, (x is the magnetic core volume fraction). The first term in Eq. (1) describes the contribution of the particles in the blocked state. Its relative contribution drops with increasing temperature, as the number of the blocked particles decreases. The $f(V)$ can be related to the distribution of blocking temperature by the linear expression $25kT_B=KV$. Therefore, one can obtain $K$ by fitting the ZFC curves using $\sigma_V=0.38$ obtained by SAXS, and the $M_S$ value obtained from the $M$ vs $H$ measured at low temperatures (keeping $M_S^{\text{core}}$ and $K$ as free fitting parameters). Figure 3 shows the reduced curve for the most diluted sample (C005) and the corresponding fit. From this analysis, $K=3.6\times10^5$ erg/cm$^3$ and $M_S^{\text{core}}=490$ emu/cm$^3$. As can be seen in Fig. 3, the superparamagnetic model is a good approach to describe the C005 sample behavior, suggesting that the possibility of particles agglomeration is not significant in that sample. In addition, this result confirms the morphological information derived from SAXS.

The coercive field, $H_C$, obtained from the $M/M_S$ vs $H$ curves measured at different temperatures is shown in Fig. 4 (at temperatures below the blocking one). The coercive field temperature behavior of systems of identical noninteracting particles with random anisotropy axes follows the well-known relation,[28]

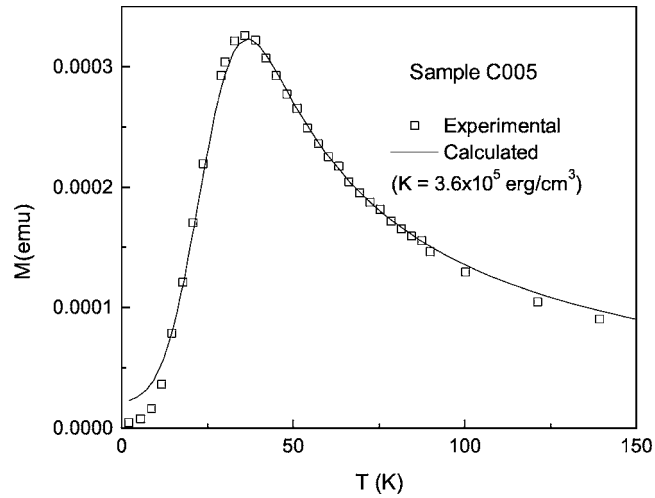


FIG. 3. The zero-field cooled curve of a C005 sample measured with $H=20$ Oe. The line is the best fit of Eq. (1) to the experimental data (symbol) using the SAXS distribution and $M_S^{\text{core}}$ and $K$ as free parameters.

$$Hc = 0.96\frac{K}{M_S^{\text{core}}}[1-(T/T_B)^{1/2}]. \qquad (2)$$

It can be inferred from Fig. 4 that the $H_C$ behavior of the samples C5 and C45 can be described by Eq. (2) at least in the low temperature range, giving $K/M_S^{\text{core}}=670$ Oe and 636 Oe, respectively. This simple approximation, however, does not hold reasonably for the powder sample. The decrease of the $H_C$ value for sample C45 compared to C5 is in agreement with the demagnetizing role played by the dipolar interaction as simulated by Kechrakos and Trohidou.[29] The $Hc$ vs $T$ trends also confirm that the only parameter change in our samples is the particle concentration. Using the $K$ value obtained from the ZFC analysis of C005 sample, we find

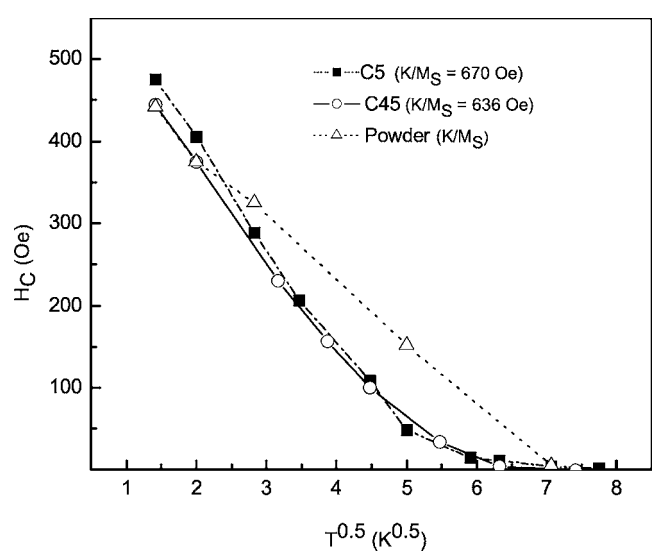


FIG. 4. $H_C$ vs $T^{0.5}$ obtained for the C5, C45, and powder samples. Similar behavior of samples C5 and C45 can be seen. In addition, these samples present a linear dependence with $T^{0.5}$ in the low temperature range. The lines serve as a guide to the eyes.

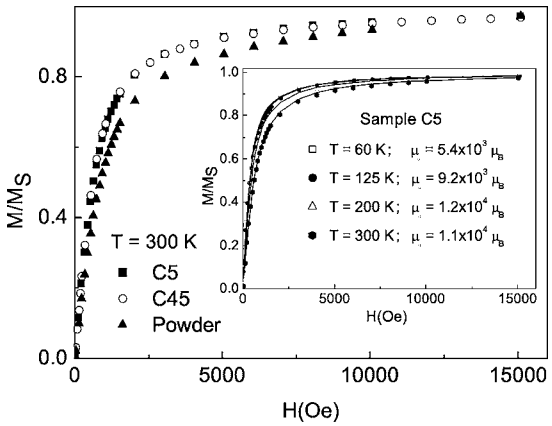


FIG. 5. The $M$ vs $H$ curves of C5, C45 and powder samples pointing out the effect of the dipolar interaction. The inset shows the C5 data as a function of temperature and the corresponding fits using the conventional superparamagnetic model showing a nice agreement but spurious $\mu$ values (these values correspond to the $\mu_a$ in the $T^*$ model).

$M_S^{\text{core}}=537$ emu/cm$^3$ and $M_S^{\text{core}}=564$ emu/cm$^3$ for samples C5 and C45. Considering the approximations involved in both fits, the results are in very good agreement with the ZFC analysis.

$M/M_S$ vs $H$ curves have been measured at several temperatures for all samples. The loops of sample C005 and C05 were strongly influenced by paraffin diamagnetism, which screens the high-field region of the measurements, and therefore those results will not be considered in the following analysis. Figure 5 shows the $M/M_S$ vs $H$ of C5, C45, and powder samples measured at 300 K showing the effect of dilution. The inset shows the evolution of $M/M_S$ vs $H$ of C5 as a function of temperature. It is important to mention that the universal curve $M/M_S$ vs $H/T$, expected in a canonical superparamagnetic system when plotting $M$ vs $H$ curves taken at different temperatures, cannot be obtained.[30] This lack of agreement is more pronounced for the powder sample, as expected due to stronger interparticle interactions.

### B. Influence of the dipolar interaction

To study in more detail the effect of interparticle interactions as function of particle concentration, we have employed the $T^*$ model.[4] In such a model, the effect of the dipolar interaction is introduced by means of a fictitious temperature, $T^*$, which is added to the actual temperature $T$ in the denominator of the Langevin function argument. This phenomenological theory can be used to relate the experimental magnetization $M$ of a set of interacting nanoparticles to their actual magnetic moment $\mu$,

$$M(H,T)=N\int_0^\infty \mu L\left(\frac{\mu H}{k(T+T^*)}\right)f(\mu)d\mu, \tag{3}$$

where $N$ is the number of particles per unit volume, $f(\mu)$ is the distribution of magnetic moments that is determined from the experimental volume distribution ($\mu=M_S^{\text{core}}V$), and $L$ is the Langevin function. It is important to remark that $T^*$ is not simply a fitting parameter. It can be related to the *rms* dipolar energy $\varepsilon_D$,

$$\varepsilon_D=kT^*=\alpha\ \mu^2/D^3, \tag{4}$$

where $\alpha$ is a constant (derived from the sum of all dipolar energy contributions), and $D$ is the average interparticle distance.[4] This is the main assumption of the $T^*$ model that considers that a dipolar field exerts a disordering and random torque to the magnetic moments of the particles, "decreasing" the ordering effect played by the applied magnetic field (similar to the effect of temperature).

Using the condition $ND^3=1$ and $M_S=N\mu$, $T^*$ can be calculated as

$$T^*=\frac{\alpha}{k}\frac{\mu^2}{D^3}=\frac{\alpha}{k}N\ \mu^2=\frac{\alpha}{k}\frac{M_S^2}{N}. \tag{5}$$

Equation (3) can be rewritten as a weighted sum of *standard* Langevin functions, but considering instead an apparent magnetic moment $\mu_a$ and an apparent particle density, $N_a$, given by,[4]

$$\mu_a=\frac{1}{1+\dfrac{T^*}{T}}\mu. \quad N_a=\left(1+\frac{T^*}{T}\right)N, \tag{6}$$

and, as a consequence,

$$M(H,T)=N_a\int_0^\infty \mu_a L\left(\frac{\mu_a H}{kT}\right)f(\mu_a)d\mu_a. \tag{7}$$

The only two fitting parameters are $N_a$ and $\mu_a$ for each temperature and $N_a$ is assumed to be independent of temperature, since $f(u_a)$ was obtained from SAXS. In this work we used the reduced form of Eq. (7), reducing the fitting parameters to a single parameter, $\mu_a$, for each temperature:

$$\frac{M(H,T)}{M_S}=\frac{\displaystyle\int_0^\infty \mu_a L\left(\frac{\mu_a H}{kT}\right)f(\mu_a)d\mu_a}{\displaystyle\int_0^\infty \mu_a f(\mu_a)d\mu_a}. \tag{8}$$

The $M/M_S$ vs $H$ curves fits for each temperature were very good in all cases (see inset in Fig. 5 for the analysis of C5 sample) and the inset of Fig. 6 shows the $\mu_a$ as a function of temperature for the three considered samples. It can be inferred from Fig. 6 an increase of $\mu_a$ with the temperature up to a maximum value, depending on sample concentration. Since all samples have the same magnetic anisotropy, this reinforces the hypothesis of the existence of a strict relationship between the dipolar interaction and the anomalous thermal behavior of $\mu_a$, commonly observed in single domain particle systems.[4]

The only required parameter to calculate the real magnetic moment $\mu$ from $\mu_a$ is $T^*$ [see Eq. (6)]. The $T^*$ can be derived from the low-field susceptibility of an interacting superparamagnetic system within the framework of this model,

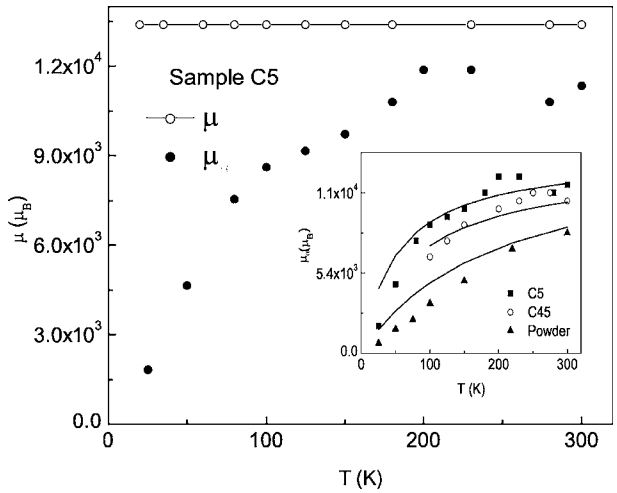


FIG. 6. $\mu_a$ and $\mu$ values as a function of temperature for C5 ($\mu$ taken constant). The inset shows the $\mu_a$ values for the three samples.

$$\chi = \frac{N\mu^2}{3k(T+T^*)}, \tag{9}$$

which, for a system with size distribution, can be expressed as[4]

$$\frac{\rho}{\chi} = 3kN\left(\frac{T}{M_S^2}\right) + 3\alpha = AT + C, \tag{10}$$

where $\rho = \langle\mu^2\rangle/\langle\mu\rangle^2 = \langle\mu_a^2\rangle/\langle\mu_a\rangle^2$, the brackets indicating the average over the values of the distribution of magnetic moments (see details in Ref. 4). $T^*$ can now be readily obtained from the ratio $C/A$ [(see Eqs. (5) and (10)]. The curve $\rho/\chi$ vs $T$ can be independently obtained from different routes, such as the high-temperature region of the ZFC-FC curves, i.e., above blocking temperature, or from the low-field region of the anhysteretic curves (average of two branches of a hysteresis loop[31]). In the present case, the $\chi(T)$ values were obtained of the linear region of the anhysteretic magnetization curves. The fit was performed in the linear region of the normalized form of Eq. (10), $\rho M_S/\chi$ vs $T$, using $M_S$ (in emu) at 20 K, and the results are presented in Table I and Fig. 7. It is interesting to note in Fig. 7 that the angular coefficient, $M_S A$, which is equal to $3k/\mu$, is similar to the three samples as it should be expected since the only variable parameter among samples is the concentration. It is important to point out, however, that $T^*$ may be underestimated by taking the normalization, $M_S$, at 20 K, but the correct trend among samples is still obtained.

TABLE I. The values of $M_S A$ and $M_S C$ derived from the fit of $\rho M_S/\chi$ vs $T$ using Eq. (10) and the resulting values of $T^*$. The $\rho$ value obtained from the SAXS volume distribution was 1.13.

| Sample | $M_S A$ | $M_S C$ | $T^*$ (K) |
|---|---|---|---|
| C5 | 3.3 | 173 | 51.7 |
| C45 | 3.5 | 266 | 76.1 |
| Powder | 3.2 | 622 | 196.1 |

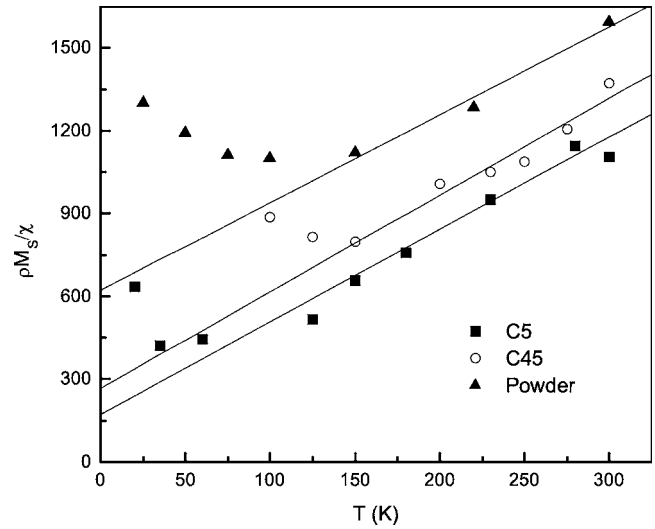


FIG. 7. The $\rho M_S/\chi$ vs $T$ graphic obtained from the linear region of the magnetization curves (magnetization under low field $H$) for the three samples. The solid lines are the best fits done to derive the $T^*$ values (see the text).

Figure 6 shows the real magnetic moment $\mu$ obtained from $\mu_a$ and $T^*$ (considering $M_S$ constant with temperature). To corroborate the analysis, the temperature dependence of the $\mu_a$ calculated by using the $T^*$ and $\mu$ are shown by lines in the inset of Fig. 6, showing a good agreement with the results obtained via the fit of $M/H$ vs $H$ curves at different temperatures.

We have also tested different approaches to fit the $M/M_S$ x $H$ curves, for example, considering $T^*$ and $\mu$ as fitting parameters, where curves taken at different temperatures are fitted simultaneously. The results and goodness of the fits were similar to the previous case. We have also tested to leave the moment distribution width as a free parameter, and it converged to the value derived from the SAXS analysis for all samples, further validating the analysis.

It is worth emphasizing that good fits using a properly weighted set of Langevin functions are not surprising, but often the obtained size distribution parameters are quite different from those obtained from direct structural measurements.[4–6,32] However, considering the $T^*$ model applied in the present work, the fitting parameters agree rather well with structural data. One can estimate the mean magnetic moment, $\langle\mu\rangle = M_S^{\text{core}} V$, by considering spherical particles, $d_{av} = 7.3$ nm, and $M_S = 537$ emu/cm$^3$ (calculated from the coercivity measurements for sample C5). This procedure leads to a value of the magnetic moment, $\langle\mu\rangle = 11802\ \mu_B$, which is rather close to the values obtained from the $T^*$ model.

## IV. CONCLUSION

In this work, spherical magnetic nanoparticles with narrow size distribution and organic capping were diluted in paraffin with different concentrations to tune interparticle dipole-dipole interactions. We clearly demonstrated that a

shift of the blocking temperature with increasing concentrations is observed when solely dipolar interactions are strengthened. Morover, to the best of our knowledge, this is the first experimental test of the $T^*$ model using a well-behaved system composed by truly isolated spherical nanoparticles with narrow size distribution. Using this model, we were able to derive the correct trends among samples and the real magnetic moment, which was in good agreement with ZFC-FC and Hc analysis. Also, different fit routes were tested, and all of them converged to very similar values, very close to those obtained from structural data. Such data and their analysis point to an adequacy of such a phenomenological model to explain the trends of the intricate macroscopic magnetic behavior of a superparamagnetic system with the presence of dipolar interactions among magnetic particles. However, further analysis should be carried out to further corroborate quantitatively the results derived from this model.

## ACKNOWLEDGMENT

Brazilian funding agencies FAPESP, CAPES, CNPq, and Brazilian Synchrotron Light Laboratory (SAXS beamline and LME) are acknowledged for their support.

*Present address: Centro Atómico Bariloche, Avenue Bustillo 9. 500(R8402AGP) San Carlos de Bariloche (RN), Argentina.

[1] L. Néel, Ann. Geophys. (C.N.R.S.) **5**, 99 (1949).
[2] X. Battle and A. Labarta, J. Phys. D **35**, R15 (2002).
[3] R. Skomski, J. Phys.: Condens. Matter **15**, R841 (2003).
[4] P. Allia, M. Coisson, P. Tiberto, F. Vinai, M. Knobel, M. A. Novak, and W. C. Nunes, Phys. Rev. B **64**, 144420 (2001).
[5] A. L. Brandl, J. C. Denardin, L. M. Socolovsky, M. Knobel, and P. Allia, J. Magn. Magn. Mater. **272-276**, 1526 (2004).
[6] H. Mamiya, I. Nakatani, T. Furubayashi, and M. Ohnuma, Trans. Magn. Soc. Jpn. **2**, 36 (2002).
[7] S. Mørup and C. Frandsen, Phys. Rev. Lett. **92**, 217201 (2004);N. J. O. Silva, L. D. Carlos, and V. S. Amaral, *ibid.* **94**, 039707 (2005);S. Morup and C. Frandsen, *ibid.* **94**, 039708 (2005);A. H. MacDonald and C. M. Canali, *ibid.* **94**, 089701 (2005);S. Morup and C. Frandsen, *ibid.* **94**, 089702 (2005).
[8] M. Knobel, W. C. Nunes, A. L. Brandl, J. M. Vargas, L. M. Socolovsky, and D. Zanchet, Physica B **354**, 80 (2004).
[9] J. L. Dormann, L. Bessais, and D. Fiorani, J. Phys. C **21**, 2015 (1988);J. L. Dormann, D. Fiorani, and E. Tronc, J. Magn. Magn. Mater. **202**, 251 (1999).
[10] W. Luo, S. R. Nagel, T. F. Rosenbaum, and R. E. Rosensweig, Phys. Rev. Lett. **67**, 2721 (1991).
[11] S. Mørup and E. Tronc, Phys. Rev. Lett. **72**, 3278 (1994).
[12] Y. Sun, M. B. Salamon, K. Garnier, and R. S. Averback, Phys. Rev. Lett. **91**, 167206 (2003);M. Sasaki, P. E. Jönsson, H. Takayama, and P. Nordblad, *ibid.* **93**, 139701 (2004).
[13] M. F. Hansen *et al.*, J. Phys.: Condens. Matter **14**, 4901 (2002).
[14] W. Kleemann, O. Petracic, C. Binek, G. N. Kakazei, Y. G. Pogorelov, J. B. Sousa, O. S. Cardos, and P. P. Freitas, Phys. Rev. B **63**, 134423 (2001).
[15] E. P. Wohlfarth, Physica B & C **86**, 852 (1977).
[16] S. Chakraverty, M. Bandyopadhyay, S. Chatterjee, S. Dattagupta, A. Frydman, S. Sengupta, and P. A. Sreeram, Phys. Rev. B **71**, 054401 (2005).
[17] J. M. Vargas, L. M. Socolovsky, G. F. Goya, M. Knobel, and D. Zanchet, IEEE Trans. Magn. **39**, 2681 (2003).
[18] D. I. Svergun, J. Appl. Crystallogr. **25**, 495 (1992).
[19] P. C. Ohara, D. V. Leff, J. R. Heath, and W. M. Gelbart, Phys. Rev. Lett. **75**, 3466 (1995).
[20] J. C. Denardin, A. L. Brandl, M. Knobel, P. Panissod, A. B. Pakhomov, H. Liu, and X. X. Zhang, Phys. Rev. B **65**, 64422 (2002).
[21] J. L. Dormann, D. Fiorani, and E. Tronc, Adv. Chem. Phys., **98**, 283 (1997).
[22] R. D. Zysler, C. A. Ramos, E. De Biasi, H. Romero, A. Ortega, and D. Fiorani, J. Magn. Magn. Mater. **221**, 37 (2000).
[23] J. García-Otero, M. Porto, J. Rivas, and A. Bunde, Phys. Rev. Lett. **84**, 167 (2000).
[24] M. Bahiana, J. P. Pereira Nunes, D. Altbir, P. Vargas, and M. Knobel, J. Magn. Magn. Mater. **281**, 372 (2004).
[25] B. V. B. Sarkissian, J. Phys.: Condens. Matter **208**, 2191 (1981).
[26] L. M. Socolovsky, F. H. Sánchez, and P. H. Shingu, Hyperfine Interact. **133**, 47 (2001).
[27] T. Bitoh, K. Ohba, M. Takamatsu, T. Shirane, and S. Chikazawa, J. Phys. Soc. Jpn. **64**, 1305 (1995).
[28] E. F. Kneller and F. E. Luborsky, J. Appl. Phys. **34**, 656 (1963).
[29] D. Kechrakos and K. N. Trohidou, Phys. Rev. B **58**, 12169 (1998).
[30] I. S. Jacobs and C. P. Bean, in *Magnetism*, edited by G. T. Rado and H. Suhl (New York, Academic Press, 1963), Vol. III, pp.271-350.
[31] P. Allia, M. Coisson, M. Knobel, P. Tiberto, and F. Vinai, Phys. Rev. B **60**, 17 12207 (1999).
[32] Q. A. Pankhurst, D. H. Ucko, L. Fernández Barquín, and R. García Calderón, J. Magn. Magn. Mater. **266**, 131 (2003).